Covalently Dye-Linked, Surface-Controlled, and Bioconjugated Organically Modified Silica Nanoparticles as Targeted Probes for Optical Imaging

Rajiv Kumar,[†] Indrajit Roy,[†] Tymish Y. Ohulchanskyy,[†] Lalit N. Goswami,[†] Adela C. Bonoiu,[†] Earl J. Bergey,[†] Kenneth M. Tramposch,[†] Anirban Maitra,[‡] and Paras N. Prasad[†,*]

[†]Institute for Lasers, Photonics, and Biophotonics, University at Buffalo, State University of New York, Buffalo, New York 14260-3000 and [‡]Department of Pathology, Johns Hopkins School of Medicine, Baltimore, Maryland 21231

ABSTRACT In this paper we report the synthesis and characterization of organically modified silica (ORMOSIL) nanoparticles, covalently incorporating the fluorophore rhodamine-B, and surface-functionalized with a variety of active groups. The synthesized nanoparticles are of ultralow size (diameter ~20 nm), highly monodispersed, stable in aqueous suspension, and retain the optical properties of the incorporated fluorophore. The surface of the nanoparticles can be functionalized with a variety of active groups such as hydroxyl, thiol, amine, and carboxyl. The carboxyl groups on the surface were used to conjugate with various bioactive molecules such as transferrin, as well as monoclonal antibodies such as anti-claudin 4 and anti-mesothelin, for targeted delivery to pancreatic cancer cell lines. *In vitro* experiments have revealed that the cellular uptake of these bioconjugated (targeted) nanoparticles is significantly higher than that of the nonconjugated ones. The ease of surface functionalization and incorporation of a variety of biotargeting molecules, combined with their observed noncytotoxicity, makes these fluorescent ORMOSIL nanoparticles potential candidates as efficient probes for optical bioimaging, both *in vitro* and *in vivo*.

KEYWORDS: ORMOSIL nanoparticles · optical imaging · bioconjugation · cellular uptake · pancreatic cancer

The advent of ceramic-based nanomaterials has revolutionized the field of medicine (in both diagnosis[1,2] and therapy[3–5]) owing to their robustness, safety, and most importantly, multimodality, that is, the ability for multiple functions.[6,7] Advantages that such macromolecular, nanoparticulate agents will have over traditional molecular agents include the following: (a) they provide a fluorescent nanoplatform upon which targeting agents (antibodies, peptides, or small molecules) can be added or substituted to suit a specific need;[8] (b) they allow for multimodality (*e.g.*, optical, magnetic resonance [MR], and radionuclide) imaging,[9] thus permitting cross-evaluation with the same nanoparticle across different imaging platforms; (c) they can be functionalized to possess both imaging and therapeutic abilities (*i.e.*, "theranostic" nanoparticles); (d) they may be designed to provide salutary benefits related to pharmacokinetics by exclusive renal excretion; (e) they are of sufficient size to permit multivalency and, therefore, the potential for higher affinity binding than standard agents; and (f) they enable imaging from the single cell level to the entire, intact organism *in vivo*. That last attribute further enables validation of the imaging marker by correlating results obtained *in vitro*, for example, relying on the optical aspects (fluorescence) of the probe, with those obtained *in vivo*, which may also rely on optical (if a near-infrared [NIR] emitting core is used), radioactive, or MR imaging.

Compared to other nanomaterials (*e.g.*, silica and iron-oxide nanoparticles, gold nanospheres/nanorods and quantum dots/rods, *etc.*), the organically modified silica (ORMOSIL) nanoparticles stand out in their versatility as an ideal platform for "building up" of multimodal "theranostic" nanoparticles. These inert, optically transparent materials can be doped with any desired fluorophore (visible/NIR), leading to the generation of robust, fluorescent nanoparticles.[10–13] They can be incorporated with bioactive molecules such as enzymes, genetic materials, and chemotherapeutic drugs, *etc.*, for a specific biological function.[14–16] In addition, the chemistry of silica provides the opportunity for a variety of surface functionalities (hydroxyl/amino/thiol/carboxyl groups),[17–20] which can be used to incorporate additional functionalities such as probes for MR/radio imaging and therapeutic and biotargeting molecules, etc.[21] Using silica nanoparticles

***Address correspondence to pnprasad@acsu.buffalo.edu.**

Received for review November 13, 2007 and accepted February 21, 2008.

Published online March 7, 2008.
10.1021/nn700370b CCC: $40.75

© 2008 American Chemical Society

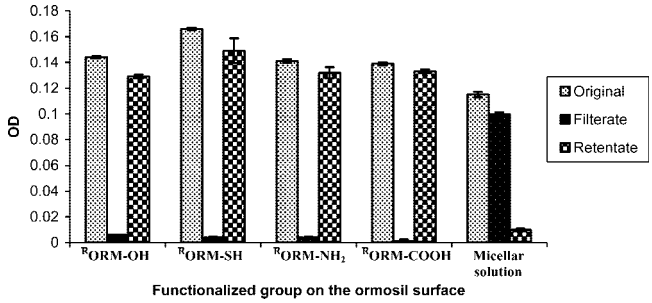

Figure 1. Release behavior of rhodamine conjugated ORMOSIL nanoparticles with different functional groups on the surface.

conjugated with fluorophores and targeting ligands, efficient optical imaging of tumor cells *in vitro* has already been demonstrated.[22,23]

In our laboratory, we have developed ORMOSIL nanoparticles for a variety of therapeutic applications, including photodymanic therapy (PDT) of cancer and gene delivery.[24–26] These nanoparticles can have a number of advantages over their unmodified counterparts. Unlike the water-in-oil microemulsion mediated synthesis reported for silica nanoparticles, these nanoparticles can be easily and reproducibly synthesized with ultralow size (diameter ≈ 20 nm) and narrow size-distribution in simple aqueous phase (oil-in-water microemulsion), where corrosive nonpolar solvents and complex purification steps such as solvent evaporation, ultracentrifugation, *etc*. can be avoided.[27] Since low size is a critical determinant toward unimpeded systemic circulation and easy infiltration to tumor and other tissues, these nanoparticles are well suited for *in vivo* applications when compared with other reported luminescent silica-based nanoparticles with bigger sizes (diameter 70 nm).[23,28,29] In addition, such materials are mesoporous and have tunable pore size, and therefore can be potentially used as vehicles for controlled, externally activated release of lipophilic therapeutic molecules such as anticancer drugs. Also, the presence of an organic group imparts a certain degree of flexibility to the otherwise rigid silica matrix, which is expected to enhance the stability of such particles against flocculation/precipitation in aqueous systems. In addition, a desired surface charge can be introduced in the organic arm of ORMOSIL, which can be used for further conjugation with diagnostic/therapeutic/biotargeting agents for the fabrication of "multimodal" nanoparticles.

Here, we report the synthesis and characterization of ORMOSIL nanoparticles, covalently conjugated with the fluorophore rhodamine (^{R}ORM) and presenting a variety of active (hydroxyl/amine/thiol/carboxyl) groups on its surface, using the oil-in-water microemulsion method. Covalent conjugation, as opposed to simple encapsulation, obviates the possibility of fluorophores being leached out of the ORMOSIL matrix in physiological fluids. The carboxyl-functionalized nanoparticles were further conjugated with a variety of bioactive molecules such as transferrin, anti-claudin 4, and anti-mesothelin, in order to demonstrate active targeting, aimed at their corresponding receptors which are overexpressed on pancreatic cancer cells/tissues.[30–33] The *in vitro* uptake of these nanoparticles with these targeting properties was found to be significantly higher than that of the nontargeted ones. Cell viability assay revealed no indication of cytotoxicity of these nanoparticles within the experimental conditions. The ease of surface functionalization and incorporation of a variety

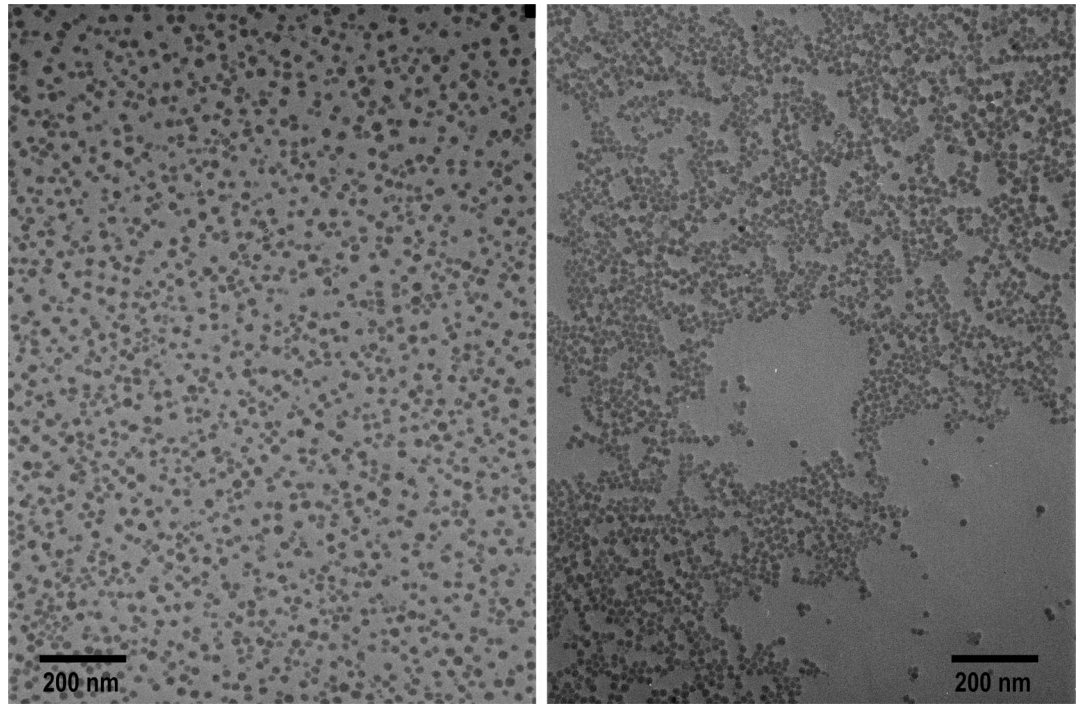

Figure 2. TEM images of ^{R}ORM-NH$_2$ and ^{R}ORM-COOH nanoparticles.

of biotargeting molecules, combined with their observed noncytotoxicity, makes these fluorescent nanoparticles potential candidates as efficient probes for optical bioimaging, both *in vitro* and *in vivo*.

RESULTS AND DISCUSSION

Figure 1 shows the relative optical densities (read at 563 nm, the long-wavelength absorbance peak for rhodamine as used here) of the filtrates and retentates, as well as the original nonfiltered samples for ^{R}Mic, ^{R}ORM-OH, ^{R}ORM-SH, ^{R}ORM-NH_2, and ^{R}ORM-COOH. From the figure, it is evident that while rhodamine-silane (RS) alone does not form any nanoparticles (*i.e.*, remains in the nonpolymerized or partially polymerized form), almost all of it is associated with the Tween-80 micellar filtrate. In contrast, ~90% of rhodamine is associated with the nanoparticles in ^{R}ORM-OH, ^{R}ORM-SH, $_{R}$ORM-NH_2, and ^{R}ORM-COOH which is collected as retentate. This indicates the high efficiency of incorporation of the fluorophore within the nanoparticles. The above synthesized nanoparticles (^{R}ORM -OH, ^{R}ORM-SH, $_{R}$ORM-NH_2, and ^{R}ORM-COOH) are highly monodispersed, with a diameter range of 20–25 nm, as determined from their TEM images (Figure 2).

To prove that rhodamine is conjugated with the nanoparticles, and not merely physically associated, we compared spin filtered rhodamine-conjugated nanoparticles against rhodamine-encapsulated nanoparticles and rhodamine/micelles (1% aqueous Tween 80) on thin layer chromatography (TLC) plates (Figure S1, Supporting Information). We observed an anticipated difference between the rhodamine-conjugated nanoparticles *versus* the rhodamine-encapsulated nanoparticles or the rhodamine/micelle preparations. As expected, rhodamine-encapsulated in nanoparticles and the rhodamine/micelles behave as free dye and run on silica-TLC plates ($R_f \approx 0.5$ in 10% methanol/dichloromethane); however, the rhodamine-conjugated with nanoparticles remain at the base. The organic phase is not able to wash away the rhodamine molecules when they are covalently linked to the nanoparticles. On the other hand, the loosely bound rhodamine molecules (in case of encapsulated in nanoparticles) can be easily extracted from the nanoparticles by organic solvents. Thus conjugation of a fluorophore with the carrier nanoparticle is necessary as this eliminates the possibility of "leakage" of the fluorophore in the free form, particularly during *in vivo* circulation.

The optical absorption and fluorescence spectra of the dispersion of the nanoparticles-conjugated rhodamine as well as the solutions of rhodamine−NHS ester and rhodamine−silane precursor are shown in Figure 3A. As one can see, the spectra are very similar; with an exception of the rhodamine−NHS ester which demonstrated a lower fluorescence emission intensity. The fluorescence quantum yield of the rhodamine−NHS ester in water was ~0.37, whereas

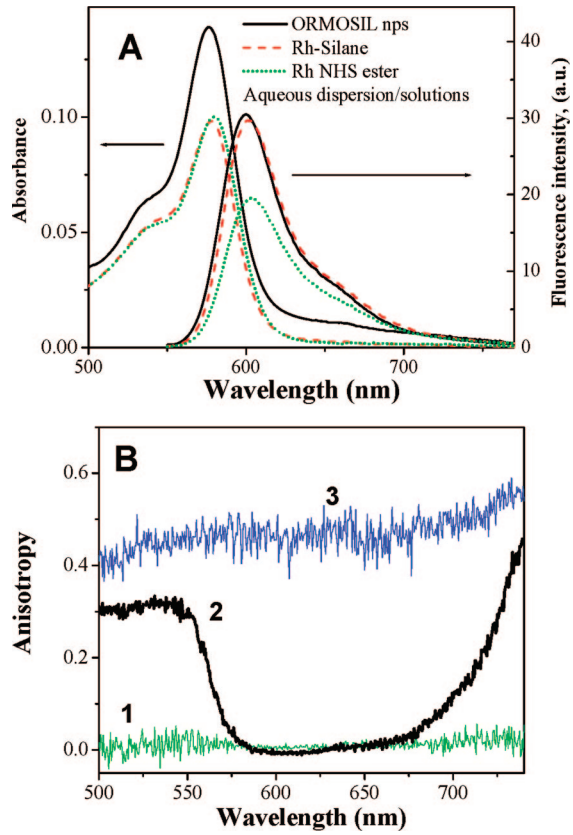

Figure 3. (A) Absorbance and fluorescence spectra of rhodamine−NHS ester (dotted), rhodamine−silane conjugate (dashed), and ORMOSIL nanoparticles with conjugated rhodamine (solid line). Fluorescence was excited with 532 nm, where optical density of rhodamine moiety was matched. (B) Fluorescence anisotropy: rhodamine−NHS ester water solution (1), rhodamine-conjugated ORMOSIL nanoparticles (2), and nonlabeled ORMOSIL nanoparticles (3).

that of same precursor when conjugated within the ORMOSIL nanoparticles was ~0.52. This increase in the fluorescence quantum yield is apparently associated with a reduction in aggregation when the rhodamine−NHS ester is converted to rhodamine−silane form with increased water solubility and conjugated within the ORMOSIL nanoparticles.

To demonstrate that the dye is indeed bound within the particle we have performed fluorescence anisotropy measurements presented in Figure 3B. The anisotropy of the fluorescence from a rhodamine−NHS ester solution and that from a suspension of fluorescently labeled ORMOSIL nanoparticles were measured. The anisotropy is defined as $r = (I_{VV} - GI_{VH})/(I_{VV} + 2GI_{VH})$, where I_{VV}, I_{VH}, I_{HV}, and I_{HH} (V and H corresponds to vertical and horizontal positions, respectively) are emission intensities for different positions of excitation and emission polarizers; the first subscript indicates the position of the excitation polarizer; the second indicates that of the emission polarizer. $G = I_{VH}/I_{HH}$ is a grating factor that must be included for correction in a monochromator.[34,35]

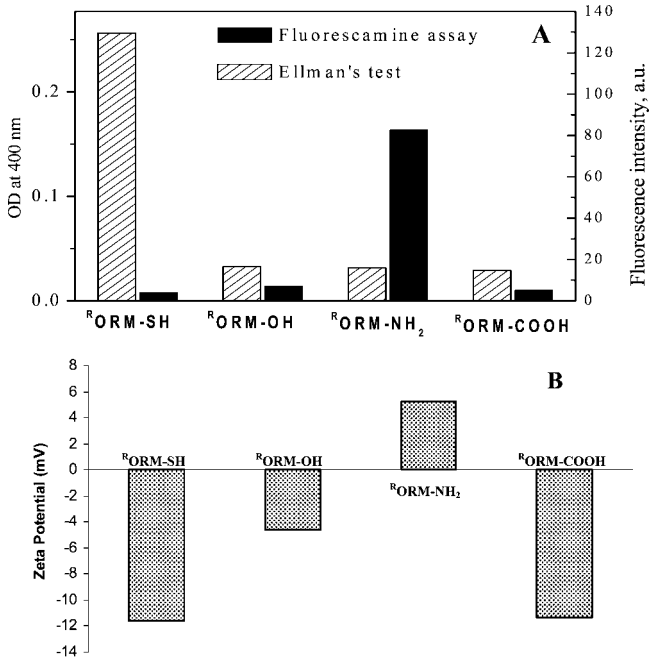

Figure 4. (A) Fluorescamine and Ellman's reagent assays with different functionalized ORMOSIL nanoparticles; (B) ζ-potential values of different surface modified rhodamine conjugated ORMOSIL nanoparticles.

The free rhodamine−NHS ester solution exhibits almost no fluorescence anisotropy. However, the fluorescence of the dye bound within the particles manifests strong anisotropy. This is understandable because of the limitation of the rotational mobility of the rhodamine molecules bound to the particles.[36] The absolute value of anisotropy, which is experimentally measured in the spectrofluorimeter, is sensitive to the excitation light that scatters off the sample. The anisotropy $r(\lambda)$ for the suspension of unlabeled ORMOSIL nanoparticles is shown as curve 3 in Figure 3B. The relative change in $r(\lambda)$ as shown in Figure 3B clearly points to the binding of the dye molecules with the particles (curve 2).

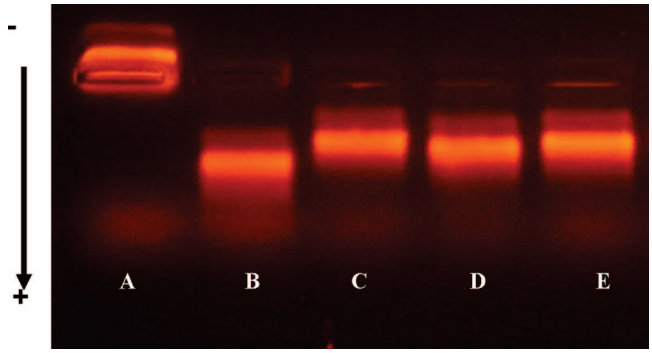

Figure 5. Agarose gel electrophoresis showing (lane A) -NH_2-terminated ORMOSIL nanoparticles (+5.35 mV*), (lane B) -COOH-terminated ORMOSIL nanoparticles (−11.31 mV*), (lane C) transferrin-conjugated ORMOSIL nanoparticles (−8.6 mV*), (lane D) anti-claudin 4-conjugated ORMOSIL nanoparticles (−7.74 mV*), and (lane E) anti-mesothelin-conjugated ORMOSIL nanoparticles (−10.75 mV*). *Numerical values denote the corresponding ζ-potential.

The surface properties of nanoparticles, modulated by the presence of free functional groups, play a critical role in their stability as aqueous dispersion, feasibility of conjugation with other bioactive/biotargeting molecules, *in vivo* pharmacodynamics, *etc*. Here, the presence of free amino groups on ^{R}ORM-NH_2 and thiol groups on ^{R}ORM-SH were confirmed by the Fluorescamine and Ellman's reagent assays, respectively (Figure 4A).[37,38]

We have also studied the surface charge of these nanoparticles by measuring their ζ-potential values. It can be seen from Figure 4B that the overall surface charge of the nanoparticles is dependent on the functional group present on their surface, being positive for ^{R}ORM-NH_2, and negative for ^{R}ORM-SH, ^{R}ORM-COOH, and ^{R}ORM-OH.[39]

To demonstrate "active targeting" of these nanoparticles to cells in culture, we have conjugated various biotargeting molecules (Transferrin, anti-claudin 4, and anti-mesothelin) with the carboxyl-terminated nanoparticles, using carbodiimide chemistry. The bioconjugation was confirmed by (a) ζ-potential measurements and (b) agarose gel electrophoresis (Figure 5). ζ-Potential measurements revealed that the net anionic charge on the nanoparticles is reduced as a result of bioconjugation, which is attributed to the partial shielding of their surface carboxyl groups by the bioconjugated proteins. The bioconjugation is also evident from the reduced mobility of the bioconjugated nanoparticles toward the positive terminal through the agarose gel (lanes B−D), as opposed to the nonconjugated one (lane A). This reduced mobility is a result of the increased overall size of the nanoparticles (data not shown), as well as a reduction in the anionic surface charge, following bioconjugation with the various proteins.

Confocal microscopy was used to study the selective uptake of the various nanoparticles by pancreatic cancer cells *in vitro*, using pre-equated amounts of the fluorophore content in each (Figure 6). It can be seen that there is a sizable difference between the intracellular uptake of the amino-terminated (panel A) and the carboxyl-terminated (panel B) nanoparticles, the uptake of the amino-terminated nanoparticles being much higher than that of the carboxyl-terminated ones. It is speculated that the favorable electrostatic interaction between the cationic amino-functionalized nanoparticles and anionic cellular membrane is responsible for this high uptake, which is not the case for the anionic carboxyl-terminated nanoparticles. However, the uptake of these carboxyl-terminated nanoparticles was dramatically enhanced upon bioconjugation with various targeting molecules. It is evident that all the three types of bioconjugated nanoparticles (with transferrin, anti-claudin 4, and anti-mesothelin) stained the cells with high efficiency (Figure 6, pan-

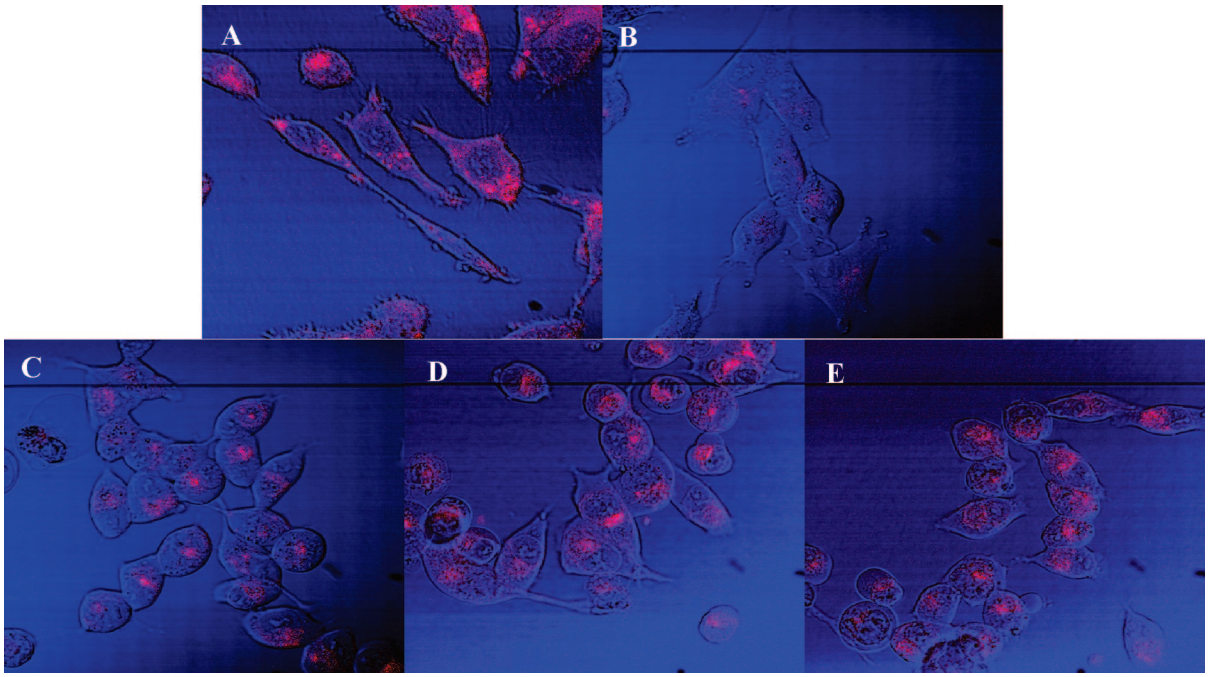

Figure 6. Confocal images of MiaPaca cells treated with ^{R}ORM-NH_2 (panel A), ^{R}ORM-COOH nanoparticles (panel B), transferrin-conjugated ^{R}ORM-COOH (panel C), anti-claudin 4-conjugated ^{R}ORM-COOH (panel D), and anti-mesothelin conjugated ^{R}ORM-COOH (panel E) nanoparticles.

els C−E). This enhanced efficiency is a result of receptor-mediated uptake of these bioconjugated nanoparticles with their corresponding receptors which are known to be overexpressed on the surface of these cells (active targeting).[28−31]

To confirm this receptor-mediated active uptake of the bioconjugated ^{R}ORM nanoparticles, comparative uptake studies of transferrin and anti-claudin 4 conjugated ORMOSIL nanoparticles were carried out in pancreatic cancer (MiaPaCa) *versus* normal (COS-1, fibroblast-like cells derived from kidneys of African green monkey) cells, using confocal microscopy. Since neither the transferrin-receptor nor claudin 4 receptors are known to be overexpressed in COS-1, no uptake of the bioconjugated nanoparticles are observed in COS-1 cells, as opposed to robust uptake observed in MiaPaCa cells (Figure S2, Supporting Information). This confirms the active or receptor-mediated nature of cellular uptake of these bioconjugated nanoparticles.

Further, the extent of cellular uptake of the various nanoparticles was quantified by determining the red (rhodamine) fluorescence from the treated cells using flow cytometry,[40] as shown in Figure 7. The logarithmic fluorescence intensity of untreated cells was set between 10^0 and 10^1, hence cells that exhibited red fluorescence intensity higher than 10^1 were taken as positively labeled with nanoparticles. The number of positively labeled cells was represented as the percentage of total cell counts in each panel. The superior uptake of the various bioconjugated nanoparticles (with anti-claudin 4, anti-mesothelin, and transferrin) is evident from the fact that more than 90% of the cells are positively labeled for rhodamine in each of these cases, as opposed to only 55.9% of positively labeled cells in the case of nonbioconjugated "nanoparticles only" control.

Finally, we have also demonstrated the absence of cytotoxicity of these nanoparticles using a cell viability

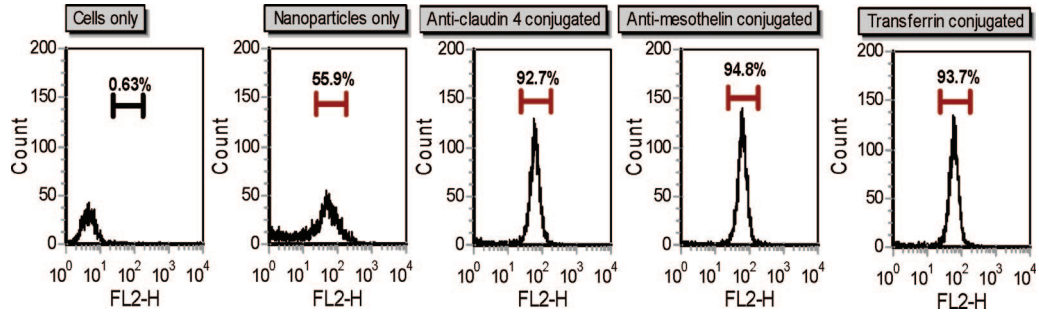

Figure 7. Flow cytometry data showing the relative uptake of various ^{R}ORM nanoparticles in MiaPaCa cells. The number of positively labeled cells was represented as the percentage of total cell counts in each panel.

(MTS) assay, with similar nanoparticle dosages as used during imaging experiments (Figure S4, Supporting Information).

CONCLUSIONS

In conclusion, we have synthesized monodispersed ORMOSIL nanoparticles, having a covalently incorporated fluorophore, with a variety of functional groups on their surface. These nanoparticles were readily conjugated to various bioactive molecules and their selective targeting to tumor cells *in vitro* is demonstrated, without any indication of cytotoxicity. Owing to the ultralow size (diameter ≈ 20 nm) of these nanoparticles, we expect that the *in vitro* tumor targeting data presented here can be successfully extended to *in vivo* tumor imaging studies. In addition, these studies underline the foundation for the development of theranostic multifunctional nanoparticles, combining the conjugation of other suitable fluorophores (*e.g.*, a NIR dye) and incorporating therapeutic molecules, drugs, for the purpose of combined diagnosis and therapy.

EXPERIMENTAL SECTION

Materials. ORMOSIL precursors vinyltriethoxysilane (VTES), aminopropyltriethoxysilane (APTES), mercaptopropyltrimethoxysilane (MPTMS), *N*′-[3-(trimethoxysilyl)-propyl]diethylenetriamine (DETA) (technical grade), the fluorophore 5(6)-carboxy-X-rhodamine *N*-succinimidyl ester (rhodamine−NHS) and transferrin were purchased from Sigma-Aldrich. Microfuge membrane-filters (NANOSEP 100K OMEGA) are a product of Pall Corporation. Anti-claudin 4 and anti-mesothelin were purchased from Invitrogen. The pancreatic cancer cell line MiaPaCa was obtained from ATCC, VA, and cultured according to instructions supplied by the vendor. Unless otherwise mentioned, all cell culture products and antibodies were obtained from Invitrogen.

Synthesis of Rhodamine-Conjugated ORMOSIL (Rhodamine−Silane) Precursor. To prepare rhodamine-conjugated silane precursor, as depicted in scheme 1, commercially available 5(6)-carboxy-X-rhodamine *N*-succinimidyl ester was used. In a typical procedure, in an oven-dried 10 mL round-bottom flask were taken rhodamine-NHS ester (10.0 mg, 0.0158 mmol), 3-aminopropyltriethoxysilane (4.19 mg, 0.0189 mmol), and neat triethylamine (10 μl). To this, anhydrous DMF (3.0 mL) was added, and the resultant mixture was stirred for 12 h at room temperature under N_2 atmosphere. The reaction mixture was concentrated under high vacuum; a crude reaction mixture thus obtained was triturated with EtOAc-hexane mixture and finally dried in a desiccator. The product was characterized using EI-MS (Figure S3, Supporting Information).

Synthesis and Purification of Rhodamine-Conjugated ORMOSIL Nanoparticles with a Variety of Surface Functional Groups. The different functional group terminated ORMOSIL nanoparticles, covalently incorporating the fluorophore rhodamine, were synthesized in the nonpolar core of an oil-in-water microemulsion system (Scheme 2). For this, three ORMOSIL precursors, rhodamine−silane (RS), VTES, and APTES or MPTMS or DETA were copolymerized. Briefly, 0.2 g of the surfactant Tween-80 and 300 μl of the cosurfactant 1-butanol, and 100 μl of DMSO were dissolved in 10 mL distilled water by magnetic stirring, forming an oil-in-water microemulsion. To this microemulsion system, 100 μl of a solution of RS (2.5 mg/ml DMSO) was dissolved, followed by addition of 100 μl of neat VTES. After stirring the reaction mixture for about an additional hour, the polymerization reaction was started by the addition of 10 μl aqueous ammonia followed by 10 μl of neat APTES, MPTMS, or DETA. The stirring was allowed to go overnight. It should be noted that in one microemulsion set none of the ORMOSIL precursors (except for RS) were added, which served as 'micellar' control (^{R}Mic). Following the synthesis of the rhodamine-conjugated ORMOSIL nanoparticles, the surfactant, cosurfactant, and other unreacted molecules were removed by dialysis against distilled water, using a cellulose membrane with a cut-off size of 12–14 kD. Following dialysis, the nanoparticles were sterile filtered and stored at 4 °C for future use.

To separate from the Tween-80 micelles, the synthesized nanoparticles were centrifuged in a microfuge membrane-filter (NANOSEP 100K OMEGA, Pall Corporation) at 14000 rpm for 30 min (spin-filtration). The Tween-80 micelles (and any nonconjugated rhodamine) flow through this membrane and are collected (filtrate). The nanoparticles are captured in the membrane of the filter and are easily redispersed in water by sonication/vortexing (retentate). A comparison of the amount of fluorophore in the filtrate and retentate fractions can be used to estimate the efficiency of incorporation of the fluorophore within the nanoparticles. All subsequent studies are carried out with the micelle-free retentate fraction of the nanoparticles.

Conversion of Amine-Terminated ORMOSIL Nanoparticles to Carboxyl Groups. The amine groups of the DETA-modified ORMOSIL nanoparticles were modified according to the method described earlier.[41] The DETA-modified ORMOSIL nanoparticles were treated with 10% succinic anhydride in DMF for 6 hrs with constant stirring. The resulting carboxylate-modified nanoparticles were dialyzed against deionized water for 14 hrs.

Conjugation of -COOH Terminated ORMOSIL Nanoparticles with Transferrin/Anti-claudin 4 and Anti-mesothelin. A 1 mL portion of stock solution of -COOH-terminated ORMOSIL nanoparticles was mixed with 25 μl of 0.1 M EDC solution and gently stirred for 30 min. Next, 5 μl of 5 mg/mL of transferrin or 5 μl of anti-claudin 4 or anti-mesothelin (0.5 mg/mL) was added into this mixture, and the mixture was incubated at room temperature for 2 h to allow the protein to covalently bond to the COOH group of the ORMOSIL nanoparticles. The conjugation was confirmed by agarose gel electrophoresis and measuring the ζ-potential values of the resulting nanoparticles.

Cell Staining Studies. For *in vitro* imaging with different functionalized ORMOSIL nanoparticles, the human pancreatic cancer cell line MiaPaCa was cultured in Dulbecco minimum essential media (DMEM) with 10% fetal bovine serum (FBS), 1% penicillin, and 1% amphotericin B. The day before nanoparticles treatment, cells were seeded in 35 mm culture dishes. On the treatment day, the cells, at a confluency of 70–80%, in serum-supplemented media were treated with the ORMOSIL nanoparticles at a

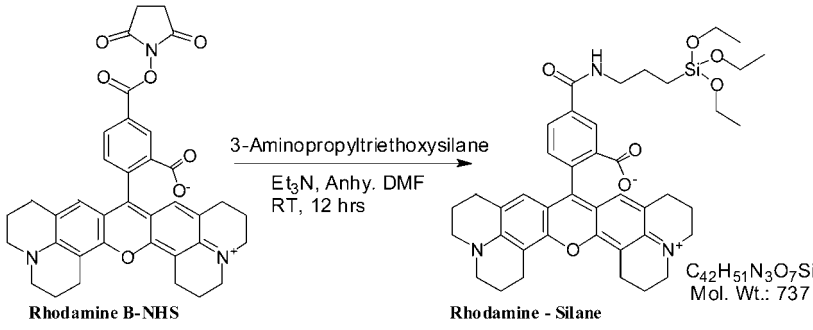

Synthesis of Rhodamine B-Silane Precursor

Scheme 1. Synthesis of rhodamine conjugated to APTES

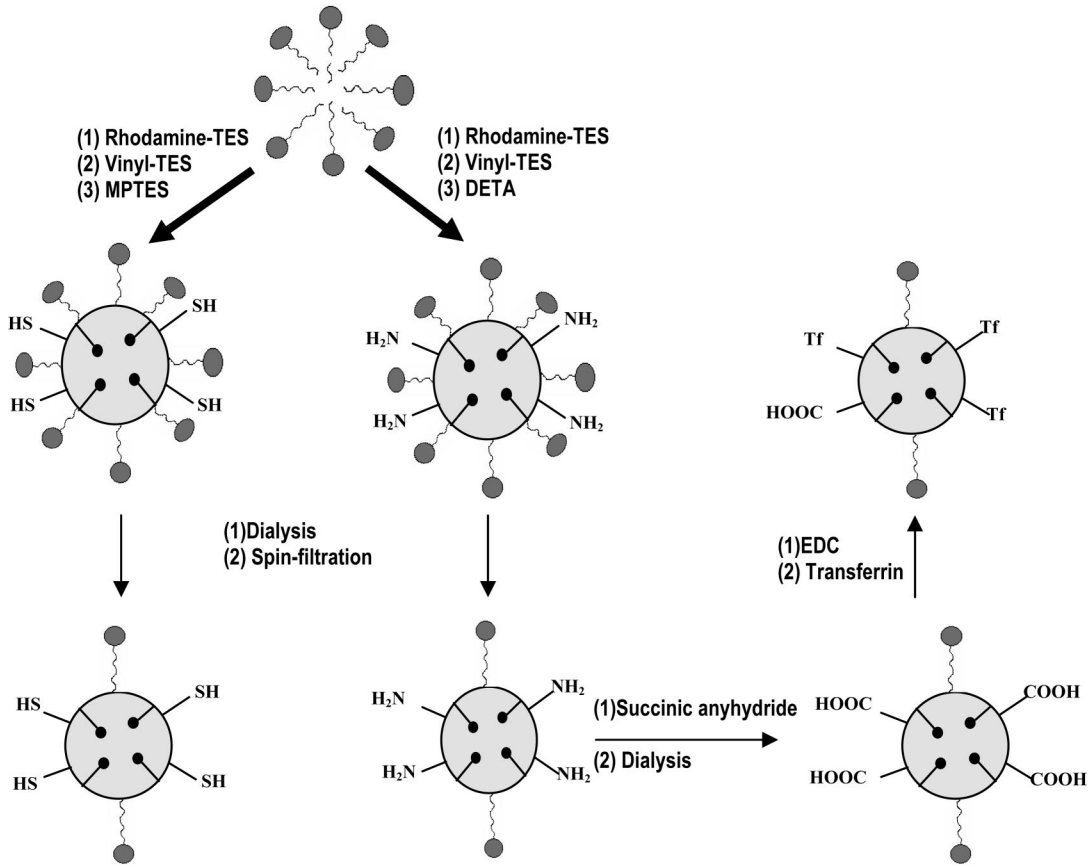

Scheme 2. Representative scheme showing the preparation of rhodamine conjugated ORMOSIL nanoparticles with different functional groups and their further conjugation to biomolecules.

specific concentration (100 μl/1 mL media) for two hours at 37 °C.

Cell Viability Assay. The MiaPaCa cells were dispensed into a 96-well flat-bottom microtiter plate (Nunc) (10000 cells/well) and allowed to attach overnight using DMEM medium with 10% FBS. Cell viability was assessed by the Cell Titer-Glo luminescent cell viability assay (Promega Corporation, Madison, WI). This assay is a homogeneous method to determine the number of viable cells in culture based on quantity of the ATP present, which signals the presence of metabolically active cells. In brief, after 4 h treatment with different bioconjugated ORMOSIL nanoparticles, media was changed, and the Cell Titer-Glo reagent was added to the cells, Each was mixed for 2 min and allowed to incubate for 10 min at room temperature. Luminescence was measured using a microplate luminometer (Bio-Tek Synergy HT microplate reader) and data ewere expressed as a percentage of the control. Tests were performed in quadruplicate. Each point represents the mean $\pm$ SD (bars) of replicates from one representative experiment.

Flow Cytometry Analysis. The cellular uptake of Rhodamine conjugated ORMOSIL nanoparticles, with and without conjugation with various targeting molecules, was quantified by flow cytometry. MiaPaCa cells were seeded at 1.0×10^6 cells per T25 flask and allowed to attach for 24 h. To determine the extent of nanoparticles uptake, the cells were incubated with 25 μl of nanoparticle solution per 1 mL serum-free medium for 2 h. Treated cells were then washed three times with phosphate-buffered saline (PBS) and then harvested by trypsinization. The red-emitting rhodamine conjugated to the ORMOSIL matrix served as the fluorescent marker to quantitatively determine their cellular uptake, and the results are analyzed by FACS Calibur flow cytometry and CellQuest Pro software (Becton Dickenson, Mississauga, CA).

Acknowledgment. This study was supported by NIH Grants CA119397 and CA104492 and the John R. Oishei Foundation. Support from the Center of Excellence in Bioinformatics and Life Sciences at the University at Buffalo is also acknowledged. Lisa A. Vathy is acknowledged for her technical help.

Supporting Information Available: Descriptions of the thin layer chromatography data, confocal microscopy data showing comparative cellular uptake of bioconjugated nanoparticles in pancreatic cancer (MiaPaCa) *versus* normal (COS-1) cell lines, MS spectra of conjugated rhodamine with APTES, and cell viability assay results. This material is available free of charge *via* the Internet at http://pubs.acs.org.

REFERENCES AND NOTES

1. Brigger, I.; Dubernet, C.; Couvreur, P. Nanoparticles in Cancer Therapy And Diagnosis. *Adv. Drug Delivery Rev.* **2002**, *54*, 631–651.
2. Alivisatos, A. P. Less is More in Medicine. *Sci. Am.* **2001**, *285*, 66–73.
3. Akerman, M. E.; Chan, W. C.; Laakkonen, P.; Bhatia, S. N.; Ruoslahti, E. Nanocrystal Targeting *in Vivo*. *Proc. Natl. Acad. Sci. U.S.A.* **2002**, *99*, 12617–12621.
4. Douglas, S. J.; Davis, S. S.; Illum, L. Nanoparticles in Drug Delivery. *Crit. Rev. Ther. Drug Carrier Syst.* **1987**, *3*, 233–261.
5. Holm, B. A.; Bergey, E. J.; De, T.; Rodman, D. J.; Kapoor, R.; Levy, L.; Friend, C. S.; Prasad, P. N. Nanotechnology in BioMedical Applications. *Mol. Cryst. Liq. Cryst.* **2002**, *374*, 589–598.
6. Prasad, P. N. *Introduction to Biophotonics*; Wiley-Interscience: New York, 2004.
7. Ferrari, M. Cancer Nanotechnology: Opportunities And Challenges. *Nat. Rev. Cancer* **2005**, *5*, 161–171.
8. Emerich, D. F. Nanomedicine - Prospective Therapeutic And Diagnostic Applications. *Expert. Opin. Biol. Ther.* **2005**, *5*, 1–5.

9. Cheng, M. M. C.; Cuda, G.; Bunimovich, Y. L.; Gaspari, M.; Heath, J. R.; Hill, H. D.; Mirkin, C. A.; Nijdam, A. J.; Terracciano, R.; Thundat, T.; Ferrari, M. Nanotechnologies for Biomolecular Detection And Medical Diagnostics. *Curr. Opin. Chem. Biol.* **2006**, *10*, 11–19.
10. Brunner, T. J.; Wick, P.; Manser, P.; Spohn, P.; Grass, R. N.; Limbach, L. K.; Bruinink, A.; Stark, W. J. In vitro Cytotoxicity of Oxide Nanoparticles: Comparison to Asbestos, Silica, And the Effect of Particle Solubility. *Environ. Sci. Technol.* **2006**, *40*, 4374–4381.
11. Ow, H.; Larson, D. R.; Srivastava, M.; Baird, B. A.; Webb, W. W.; Wiesner, U. Bright and Stable Core-Shell Fluorescent Silica Nanoparticles. *Nano Lett.* **2005**, *5*, 113–117.
12. Zhao, X.; Tapec-Dytioco, R.; Tan, W. Ultrasensitive DNA Detection Using Highly Fluorescent Bioconjugated Nanoparticles. *J. Am. Chem. Soc.* **2003**, *125*, 11474–11475.
13. Zhao, X.; Hilliard, L. R.; Menchery, S. J.; Wang, Y.; Bagwe, R. P.; Jin, S.; Tan, W. A Rapid Bioassay for Single Bacterial Cell Quantitation Using Bioconjugated Nanoparticles. *Proc. Natl. Acad. Sci. U.S.A.* **2004**, *101*, 15027–15032.
14. Jain, T. K.; Roy, I.; De, T. K.; Maitra, A. N. Nanometer Silica Particles Encapsulating Active Compounds: A Novel Ceramic Drug Carrier. *J. Am. Chem. Soc.* **1998**, *120*, 11092–11095.
15. Cordek, J.; Wang, X.; Tan, W. Direct Immobilization of Glutamate Dehydrogenase on Optical Fiber Probes for Ultrasensitive Glutamate Detection. *Anal. Chem.* **1999**, *71*, 1529–1533.
16. Fang, X. H.; Liu, X.; Schuster, S.; Tan, W. Designing a Novel Molecular Beacon for Surface-Immobilized DNA Hybridization Studies. *J. Am. Chem. Soc.* **1999**, *121*, 2921–2922.
17. Huh, S.; Wiench, J. W.; Yoo, J.-C.; Pruski, M.; Lin, V. S.-Y. Organic Functionalization and Morphology Control of Mesoporous Silicas via a Co-Condensation Synthesis Method. *Chem. Mater.* **2003**, *15*, 4247–4256.
18. Walcarius, A.; Etienne, M.; Lebeau, B. Rate of Access to the Binding Sites in Organically Modified Silicates. 2. Ordered Mesoporous Silicas Grafted with Amine or Thiol Groups. *Chem. Mater.* **2003**, *15*, 2161–2173.
19. Cagnol, F.; Grosso, D.; Sanchez, C. A General One-pot Process Leading to Highly Functionalised Ordered Mesoporous Silica Films. *Chem. Commun.* **2004**, 1742–1743.
20. Han, L.; Sakamoto, Y.; Terasaki, O.; Li, Y.; Che, S. Synthesis of Carboxylic Group Functionalized Mesoporous Silicas (CFMSs) with Various Structures. *J. Mater. Chem.* **2007**, *17*, 1216–1221.
21. Sharma, P.; Brown, S.; Walter, G.; Santra, S.; Moudgil, B. Nanoparticles for Bioimaging. *Adv. Colloid Interface Sci.* **2006**, *123–126*, 471–485.
22. Santra, S.; Liesenfeld, B.; Dutta, D.; Chatel, D.; Batich, C. D.; Tan, W.; Moudgil, B. M.; Mericle, R. A. Folate Conjugated Fluorescent Silica Nanoparticles for Labeling Neoplastic Cells. *J. Nanosci. Nanotechnol.* **2005**, *5*, 899–904.
23. Santra, S.; Yang, H.; Dutta, D.; Stanley, J. T.; Holloway, P. H.; Tan, W.; Moudgil, B. M.; Mericle, R. A. Rapid And Effective Labeling of Brain Tissue Using TAT-conjugated CdS:Mn/ZnS quantum Dots. *Chem. Commun. (Cambridge)* **2005**, *25*, 3144–3146.
24. Bharali, D. J.; Klejbor, I.; Stachowiak, E. K.; Dutta, P.; Roy, I.; Kaur, N.; Bergey, E. J.; Prasad, P. N.; Stachowiak, M. K. Organically Modified Silica Nanoparticles: A Nonviral Vector for *in Vivo* Gene Delivery And Expression in the Brain. *Proc. Natl. Acad. Sci. U.S.A.* **2005**, *102*, 11539–11544.
25. Roy, I.; Ohulchanskyy, T. Y.; Bharali, D. J.; Pudavar, H. E.; Mistretta, R. A.; Kaur, N.; Prasad, P. N. Optical Tracking Of Organically Modified Silica Nanoparticles As DNA Carriers: A Nonviral, Nanomedicine Approach For Gene Delivery. *Proc. Natl. Acad. Sci. U.S.A.* **2005**, *102*, 279–284.
26. Roy, I.; Ohulchanskyy, T. Y.; Pudavar, H. E.; Bergey, E. J.; Oseroff, A. R.; Morgan, J.; Dougherty, T. J.; Prasad, P. N. Ceramic-Based Nanoparticles Entrapping Water-Insoluble Photosensitizing Anticancer Drugs: A Novel Drug-Carrier System for Photodynamic Therapy. *J. Am. Chem. Soc.* **2003**, *125*, 7860–7865.
27. Das, S.; Jain, T. K. Maitra, A. N. Inorganic-Organic Hybrid Nanoparticles from *n*-Octyl Triethoxy Silane. *J. Colloid Interface Sci.* **2002**, *252*, 82–88.
28. Davis, S. S. Biomédical Applications of Nanotechnology — Implications for Drug Targeting and Gene Therapy. *Trends Biotechnol.* **1997**, *15*, 217–224.
29. Burns, A.; Sengupta, P.; Zedayko, T.; Baird, B.; Wiesner, U. Core/Shell Fluorescent Silica Nanoparticles for Chemical Sensing: Towards Single-Particle Laboratories. *Small* **2006**, *2*, 723–726.
30. Jiang, W.; Singhal, A.; Zheng, J.; Wang, C.; Chan, W. C. W. Optimizing the Synthesis of Red- to Near-IR-Emitting CdS-Capped $CdTe_xSe_{1-x}$ Alloyed Quantum Dots for Biomedical Imaging. *Chem. Mater.* **2006**, *18*, 4845–4854.
31. McCarthy, D. M.; Maitra, A.; Argani, P.; Rader, A. E.; Faigel, D. O.; Van Heek, N. T.; Hruban, R. H.; Wilentz, R. E. Novel Markers of Pancreatic Adenocarcinoma in Fine-Needle Aspiration: Mesothelin and Prostate Stem Cell Antigen Labeling Increases Accuracy in Cytologically Borderline Cases. *Appl. Immunohistochem. Mol. Morphol.* **2003**, *11*, 238–243.
32. Jhala, N.; Jhala, D.; Vickers, S. M.; Eltoum, I.; Batra, S. K.; Manne, U.; Eloubeidi, M.; Jones, J. J.; Grizzle, W. E. Biomarkers in Diagnosis of Pancreatic Carcinoma in Fine-Needle Aspirates: A Translational Research Application. *Am. J. Clin. Pathol.* **2006**, *126*, 572–579.
33. Nichols, L. S.; Ashfaq, R.; Iacobuzio-Donahue, C. A. Claudin 4 Protein Expression in Primary and Metastatic Pancreatic Cancer Support for Use as a Therapeutic Target. *Am. J. Clin. Pathol.* **2004**, *121*, 226–230.
34. Lakowicz, J. R. *Principles of Fluorescence Spectroscopy*; Plenum Press: New York, 1983.
35. White, C. E.; Argauer, R. J. *Fluorescence Analysis-A Practical Approach*; Marcel Dekker: New York, 1970.
36. Sahoo, Y.; Goodarzi, A.; Swihart, M. T.; Ohulchanskyy, T. Y.; Kaur, N.; Furlani, E. P.; Prasad, P. N. Aqueous Ferrofluid of Magnetite Nanoparticles: Fluorescence Labeling and Magnetophoretic Control. *J. Phys. Chem. B* **2005**, *109*, 3879–3885.
37. Ellman, G. L. Tissue Sulfhydryl Groups. *Arch. Biochem. Biophys.* **1959**, *82*, 70–77.
38. Lai, C. Y. Detection of Peptides by Fluorescence Methods. *Methods Enzymol.* **1977**, *47*, 236–243.
39. Butterworth, M. D.; Corradi, R.; Johal, J.; Maeda, S.; Lascelles, S. F.; Armes, S. P. Zeta Potential Measurements on Conducting Polymer-Inorganic Oxide Nanocomposite Particles. *J. Colloid Interface Sci.* **1995**, *174*, 510–517.
40. Chung, T.; Wu, S.; Yao, M.; Lu, C.; Lin, Y.; Hung, Y.; Mou, C.; Chen, Y.; Huang, D. The Effect of Surface Charge on the Uptake and Biological Function of Mesoporous Silica Nanoparticles in 3T3-L1 Cells and Human Mesenchymal Stem Cells. *Biomaterials* **2007**, *28*, 2959–2966.
41. Qhobosheane, M.; Santra, S.; Zhang, P.; Tan, W. Biochemically Functionalized Silica Nanoparticles. *Analyst* **2001**, *126*, 1274–1278.